

Universal scaling in the Knight-shift anomaly of the doped periodic Anderson model

M. Jiang^{1,*} and Yi-feng Yang^{2,3,4,†}

¹*Institute for Theoretical Physics, ETH Zurich 8092, Switzerland*

²*Beijing National Laboratory for Condensed Matter Physics and Institute of Physics, Chinese Academy of Sciences, Beijing 100190, China*

³*Collaborative Innovation Center of Quantum Matter, Beijing 100190, China*

⁴*School of Physical Sciences, University of Chinese Academy of Sciences, Beijing 100190, China*

(Received 3 February 2017; revised manuscript received 4 June 2017; published 30 June 2017)

We report a dynamical cluster approximation investigation of the doped periodic Anderson model to explain the universal scaling in the Knight-shift anomaly predicted by the phenomenological two-fluid model and confirmed in many heavy-fermion compounds. We calculate the quantitative evolution of the orbital-dependent magnetic susceptibility and reproduce correctly the two-fluid prediction in a large range of doping and hybridization. Our results confirm the presence of a temperature/energy scale T^* for the universal scaling and show distinctive behaviors of the Knight-shift anomaly in response to other “orders” at low temperatures. However, comparison with the temperature evolution of the calculated resistivity and quasiparticle spectral peak indicates a different characteristic temperature from T^* , in contradiction with the experimental observation in CeCoIn₅ and other compounds. This reveals a missing piece in the current model calculations in explaining the two-fluid phenomenology.

DOI: [10.1103/PhysRevB.95.235160](https://doi.org/10.1103/PhysRevB.95.235160)

I. INTRODUCTION

The NMR Knight-shift anomaly has been detected in a few families of materials, including the cuprates [1–3], heavy-fermion compounds CeCu₂Si₂, UPt₃, and URu₂Si₂ [4,5], and most recently iron-based superconductors AFe₂As₂ ($A = \text{K, Rb, Cs}$) [6]. As a ubiquitous non-Fermi liquid behavior in correlated systems, it manifests itself as the breakdown of the proportionality between the Knight shift and magnetic susceptibility as seen in normal Fermi liquids. For example, in the CeMIn₅ ($M = \text{Rh, Ir, or Co}$) class of heavy-fermion materials [7–9], the Knight shift K is proportional to the susceptibility at high temperatures. However, this simple relation fails below a material-dependent crossover temperature $T^* \sim 10\text{--}100$ K, which reflects the onset of lattice coherence or hybridization between conduction electrons and localized f electrons. More interestingly, the Knight-shift anomaly has been observed to obey a universal scaling in a particular temperature regime across a dozen heavy-fermion materials, which has attracted considerable attention [10] among various exotic behaviors of heavy-electron materials.

Theoretically, the Knight-shift anomaly has been argued to be due to a temperature-dependent hyperfine interaction [11] or the crystal field occupations of the $4f$ ($5f$) electrons in the rare-earth or actinide ions [12]. However, these developments have been criticized because of the much higher energy scale of the hyperfine coupling compared with the Kondo and crystal field interactions [13]. To understand diverse non-Fermi liquid behaviors observed in heavy-electron materials including the universality of the Knight-shift anomaly, a phenomenological two-fluid theory has been developed as a promising framework [14–19]. Specifically, this two-fluid model argues that below a material-dependent coherence temperature, T^* , an itinerant heavy-electron Kondo liquid, which displays non-Fermi liquid

scaling behavior, emerges as the localized f electrons collectively hybridize with the conduction electrons. This emergent Kondo liquid coexists with a spin liquid formed by the lattice of local moments of f electrons whose magnitude is reduced by the hybridization. Below T^* both the residual unhybridized local moments and the emergent Kondo liquid contribute to the Knight shift but with different weights so that the Knight shift is no longer proportional to the total susceptibility. Moreover, the relative weight of the local moments is continuously reduced with decreasing temperature whereas the weight of the Kondo liquid increases. These two components compete over a broad range of temperatures below T^* until the onset of either long-range order antiferromagnetism or superconductivity as ground states [14–20]. Although the intertwined two-fluid picture has gained much interest in accounting for several anomalous heavy-fermion properties, a minimal microscopic model that can clarify the nature of the two fluids and provide a comprehensive and quantitative understanding is still lacking [18].

To this end, one of us (M.J.) has performed a determinant quantum Monte Carlo (DQMC) simulation to gain some insight into the universal scaling behavior of the Knight-shift anomaly reported in experiments and the two-fluid theory [21]. That previous work confirmed the expectation that the different temperature evolution of orbital-dependent magnetic susceptibilities plays a key role [22]. They were able to derive the universal behavior of the Knight-shift anomaly below a crossover temperature T^* , in qualitative agreement with experiments and the two-fluid prediction. However, while this provides the first theoretical support of the Kondo liquid scaling, the calculations are limited to the half-filled periodic Anderson model (PAM) due to the notorious sign problem in DQMC simulations. This is in contrast with the metallic nature of the usual heavy-fermion systems. For example, in a recent study, the particular fillings $\langle n_f \rangle \sim 1, \langle n_c \rangle \sim 0.9$ were used for the Ce-115 family of heavy-fermion materials to investigate the d -wave superconductivity in the frustrated PAM [23]. It is therefore necessary to study the PAM away from the half filling.

*jiangmi@itp.phys.ethz.ch

†yifeng@iphy.ac.cn

The paper is organized as follows: Section II discusses the PAM Hamiltonian and dynamical cluster approximation (DCA) methods including the calculation of magnetic susceptibilities. Section III first provides a brief overview of the NMR Knight-shift anomaly and then illustrates its occurrence in the doped PAM from DCA simulations. Section IV focuses on our key results, namely the universal scaling of the Knight-shift anomaly in terms of both hybridization and doping level. Section V examines the spectral properties and quasiparticle scattering rate and compares their behavior with the Knight-shift anomaly. Section VI summarizes our results.

II. MODEL AND METHODOLOGY

Here we extend our previous investigation to the doped system by means of the dynamical cluster approximation (DCA) [24,25]. Absent the severe sign problem, the DCA allows us to explore how the universal scaling behavior observed in the half-filled PAM [21] evolves in hole-doped systems. In the past decades, the PAM has been extensively studied via dynamical mean field theory (DMFT) and its various extensions, e.g., the DCA and cellular DMFT, aiming to explore its phase diagram [26,27], d -wave superconductivity [23], Mott metal-insulator transition [28–30], strange metallicity [31], existence of ferromagnetism [32], charge order [33], or generalized versions of the PAM, for example, in the presence of disorder [34], attractive interaction [35], or triangular lattices [36].

The PAM on a square lattice is conventionally believed to capture the essential physics of heavy-fermion materials via a lattice of two orbitals of electrons, one of which is strongly correlated f electrons that hybridize with the conduction electrons. The Hamiltonian reads as

$$\begin{aligned} \mathcal{H} = & -t \sum_{\langle ij \rangle, \sigma} (c_{i\sigma}^\dagger c_{j\sigma} + c_{j\sigma}^\dagger c_{i\sigma}) - V \sum_{i\sigma} (c_{i\sigma}^\dagger f_{i\sigma} + f_{i\sigma}^\dagger c_{i\sigma}) \\ & + U \sum_i \left(n_{i\uparrow}^f - \frac{1}{2} \right) \left(n_{i\downarrow}^f - \frac{1}{2} \right) \\ & - \sum_{i\sigma} (\mu_c n_{i\sigma}^c + \mu_f n_{i\sigma}^f), \end{aligned} \quad (1)$$

which is same as the model employed in our previous work [21]. For more details on the relevant basic physics of the PAM and extensive review of another closely related Kondo lattice model, we refer the reader to Refs. [21,37]. $c_{i\sigma}^\dagger$ ($c_{i\sigma}$) and $f_{i\sigma}^\dagger$ ($f_{i\sigma}$) are creation (annihilation) operators for the conduction and local f electrons on site i with spin σ , respectively. $n_{i\sigma}^{c,f}$ are the associated number operators. t is the hopping parameter of the conduction electrons on nearest-neighbor sites $\langle ij \rangle$ of a square lattice, U the local repulsive interaction in the f orbital, and V the hybridization between the conduction and f electrons. $\mu_{c,f}$ denotes the orbital-dependent chemical potential. $t = 1$ sets the energy scale throughout the paper.

We remark that differently from the model settings in [23], here we adopt the fixed $\langle n_c \rangle \sim 1$ by taking the chemical potential for the conduction electron to be $\mu_c = 0$, while the f -electron orbital is doped with varying occupancy spanning from the Kondo regime ($\langle n_f \rangle \approx 1$) to the mixed-valence

regime ($\langle n_f \rangle < 1$). This is done via tuning an ‘‘artificially’’ orbital-dependent chemical potential $\mu_{c,f}$ in order to explicitly examine the impact of f -orbital occupancy, which is difficult to be realized if we simply fix the total occupancy via a ‘‘global’’ chemical potential $\mu = \mu_c = \mu_f$. In this way, we focus on the doping effects in the f orbital on the Knight-shift anomaly and its universality in terms of temperature and doping level. We note that $\langle n_c \rangle \sim 1$ resides in a special situation where the Van Hove singularity in the density of states of the conduction electrons in a tight-binding model such as the PAM with nearest-neighbor hopping in a square lattice may play a role. This allows us to compare directly with previous results obtained using DQMC where we had both $n_c = 1$ and $n_f = 1$. On the other hand, we found that the essential physics is not altered for more generic cases, e.g., with a fixed total occupancy in spite of the charge redistribution between conduction and f electrons.

As an extension of the dynamical mean field theory (DMFT) [38], the DCA represents the bulk lattice problem by a finite number of cluster degrees of freedom embedded in a self-consistent mean-field host via a coarse-graining procedure of the Green’s function, in which the Brillouin zone is divided into N_c patches and the self-energy is assumed to be constant on these patches. In this way, the DCA deals with all correlations within the cluster, while the longer range correlations outside the cluster are described in the mean-field level. This gives an approximation of the thermodynamic limit and the exact solution of the lattice model can be reproduced in the limit of infinite cluster size. In practice, the most time-consuming part of the DCA self-consistent loop is the cluster solver, which includes either perturbative techniques such as the fluctuation-exchange approximation or nonperturbative techniques such as quantum Monte Carlo (QMC) or exact diagonalization. One widely used approach is the continuous-time QMC (CT-QMC), which is based on a diagrammatic expansion of the partition function to all orders [39]. We will adopt a particular version of CT-QMC, namely the continuous-time auxiliary-field (CT-AUX) algorithm, which is based on an interaction expansion combined with an auxiliary-field decomposition of the interaction vertices owing to its accuracy and efficiency [40].

For later usage, we mention that the local magnetic susceptibility is calculated in the CT-AUX cluster solver after achieving the DCA self-consistency as

$$\chi_{\alpha\beta} = \frac{1}{N_c} \sum_i \int_0^\beta d\tau ([n_{i\uparrow}^\alpha(\tau) - n_{i\downarrow}^\alpha(\tau)] [n_{i\uparrow}^\beta(0) - n_{i\downarrow}^\beta(0)]) \quad (2)$$

with α, β denoting the conduction- and f -electron orbitals in the PAM, respectively. In principle, because the self-consistency in the DCA is achieved only at the single-particle level, e.g., for self-energy, the two-particle coarse-grained quantities such as \mathbf{q} -dependent charge/spin susceptibility are not identical to those of the cluster [24]. In fact, it is much more involved and time-consuming to calculate the two-particle quantities within the DCA [24,25] and recently developed DCA+ algorithm [41,42]. However, the local cluster quantities such as $\chi_{\alpha\beta}$ presented here are identical to the local lattice ones. We emphasize that in our simulations the Knight-shift

anomaly usually occurs at relatively high temperatures, where the local susceptibilities do not differ much from their uniform ($\mathbf{q} = 0$) counterpart, which implies that the DCA cluster size plays a minor role. For the same reason, it is reasonable that the correlation strength U does not play a significant role either. Therefore, we focus on the particular parameters: $U/t = 4, N_c = 16$. We have confirmed that other U, N_c , and even different band structures, e.g., finite next-nearest-neighbor hoppings t' for conduction electrons and/or hybridization between orbitals, do not modify the results throughout the paper qualitatively.

III. NMR KNIGHT-SHIFT ANOMALY

The hyperfine interactions coupling the nuclear spins \vec{I} to the electron spins \vec{S} significantly perturb the nuclear spins, which enables the nuclei to probe the susceptibility of the electron quasiparticles [22]. Specifically, this is reflected in the Knight shift that measures the percentage shift of the nuclear magnetic resonance (NMR) frequency from that of an isolated nucleus. In real materials, the hyperfine coupling is generally not isotropic but rather a tensor quantity $\mathcal{H}_{\text{hyp}} = \vec{I} \cdot \sum_i \mathbb{A}_i \cdot \vec{S}_i$ so that the Knight shift also has a tensor form $\mathbb{K} = \mathbb{A} \cdot \chi$, where \mathbb{A}_i is the hyperfine interaction matrix and χ is the magnetic susceptibility of the electrons. Note that in those systems with local moments such as rare-earth materials, the hyperfine coupling can be both on-site coupling to itinerant electron spins \vec{S}_i^c and transferred coupling to localized electron spins \vec{S}_i^f , the latter of which plays an important role in materials with localized electrons. For the nucleus located at the site of the local moment such as lanthanide and actinide atoms, the on-site hyperfine coupling can be so large that the fast relaxation rate results in difficulty in detecting spin echo [22]. Therefore, the transferred hyperfine coupling of ligand nuclei to their neighboring local moments is often more useful. From now on, we only consider the nuclear spins on the ligand sites and rewrite the hyperfine coupling as

$$\mathcal{H}_{\text{hyp}} = \vec{I}_i \cdot (A\vec{S}_i^c + B\vec{S}_i^f), \quad (3)$$

where A denotes the on-site hyperfine interaction with the conduction-electron spin and B is a transferred hyperfine interaction with the f -electron spin. Note that the tensor notation is dropped for simplicity. If the electron spins are polarized via an external magnetic field H , then $S_i^c = (\chi_{cc} + \chi_{cf})H$ and $S_i^f = (\chi_{cf} + \chi_{ff})H$, where $\chi_{cc}, \chi_{cf}, \chi_{ff}$ denote three components of the susceptibilities, so that the total susceptibility and Knight shift are

$$\begin{aligned} \chi(T) &= \chi_{cc}(T) + 2\chi_{cf}(T) + \chi_{ff}(T), \\ K(T) &= A\chi_{cc}(T) + (A+B)\chi_{cf}(T) + B\chi_{ff}(T). \end{aligned} \quad (4)$$

Apparently the normal Fermi liquid behavior $K \sim \chi$ is reproduced if $A = B$. Generally, $A \neq B$ and the three types of susceptibilities can have quite different temperature evolutions. Hence, in a range of temperature the Knight shift will not be proportional to susceptibility, namely the emergence of the Knight-shift anomaly. Experimentally, its occurrence below a material-dependent temperature scale T^* has been observed in a few families of heavy-electron materials [4,5,22].

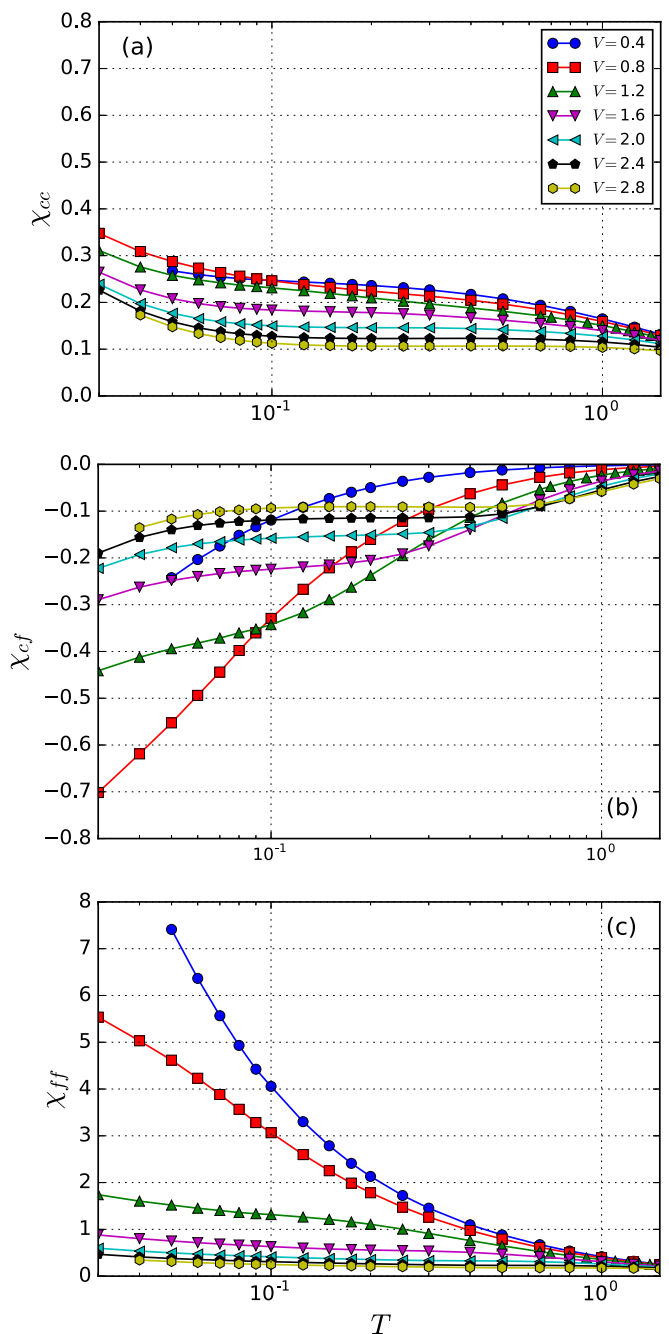


FIG. 1. Distinct temperature evolution of three types of local magnetic susceptibility for $\langle n_f \rangle = 0.9$ implies the emergence of the Knight-shift anomaly.

Theoretically, as argued in the two-fluid theory [14–18], T^* corresponds to the coherence temperature of the Kondo lattice below which the local moment and itinerant degrees of freedom become entangled and the heavy-electron Kondo fluid begins to emerge. Our previous work in the half-filled PAM [21] also numerically illustrated the existence of this coherence temperature scale. The purpose of the present paper is to show that all essential properties on the Knight-shift anomaly reported in [21] persist in the more general doped systems.

Figure 1 provides evidence of the distinct temperature evolutions of three types of susceptibilities χ_{cc} , χ_{cf} , and χ_{ff} for varying hybridization V , which signifies the possibility of the Knight-shift anomaly. Although the present study focuses on the relatively high temperature regime, namely $T/t \gtrsim 0.1$, due to the scale of the crossover temperature T^* discussed later, it is informative to discuss the whole temperature evolution of the susceptibilities. For weak hybridization (small V), the conduction electrons only weakly interact with the f -electron moments so that χ_{cc} is expected to exhibit a T -independent Pauli behavior at low temperatures. However, Fig. 1(a) displays a gradual increase with lowering temperature. In fact, even the flatness of $\chi_{cc}(T)$ anticipated for strong hybridization at low temperature disappears. This issue was attributed to the Van Hove singularity in the density of states associated with the half-filled conduction band [21]. Here the lack of T -independent χ_{cc} in the doped PAM stems from both the Van Hove singularity and overcomplete screening of f -electron local moments ($\langle n_c \rangle = 1.0$, $\langle n_f \rangle = 0.9$). Appendix A includes more discussions and comparison between DQMC and DCA results. Figure 1(b) shows the behavior of the interorbital susceptibility χ_{cf} , which is negative due to the antialignment between the conduction- and f -electron spins. As expected, a stronger hybridization leads to a larger $|\chi_{cf}|$ at the high-temperature regime. However, lowering T induces a nonmonotonic evolution of $\chi_{cf}(V)$ with the critical V around the quantum critical hybridization separating f -electron antiferromagnetism and c - f singlet phases, which also occurs for $\langle n_c \rangle = \langle n_f \rangle = 1.0$ [21]. Naturally, the small $|\chi_{cf}|$ originates from the weak hybridization at small V and the constraint due to the singlet formation at large V . Figure 1(c) displays the Curie-like divergence of χ_{ff} for weak hybridization, while stronger hybridization induces antialignment between c - f electron spins to form spin singlets, as manifested in the gradual flatness of the temperature evolution of χ_{ff} .

With the temperature evolution of χ_{cc} , χ_{cf} , and χ_{ff} , we can plot K versus χ with T as an implicit parameter, namely the Clogston-Jaccarrino plot [43]. Note that experimentally the Knight shift and magnetic susceptibility can be measured independently. If there is only a single spin component that gives rise to the magnetic susceptibility, then the data will form a straight line, which is not generic in the PAM with two orbitals. We remark that, without loss of generality, the hyperfine couplings are chosen as $A = 0.2$ and $B = 1.0$ throughout the paper [44]. For large enough hybridization V in the half-filled PAM [21], the curves of $K(\chi)$ show counterclockwise turnaround with decreasing temperature, which originates from the peak structure of the total susceptibility $\chi(T)$. Figure 2 illustrates that this feature persists in the doped PAM for $V/t \gtrsim 1.2$ but with a second clockwise turnaround, which is due to the continual increase of the total susceptibility in Fig. 3 at lower temperature. The peak value of total susceptibility decreases with increasing V , which leads to the compression of the $K(\chi)$ curve towards the origin. Note that experimentally both clockwise and counterclockwise of traversal have been observed, depending on the particular values and signs of the hyperfine coupling tensors \mathbb{A} and \mathbb{B} , whose determination are nontrivial in practice [22].

As done in the half-filled PAM [21] and experimentally [5], the high-temperature regime of $K(\chi)$ can be fitted with

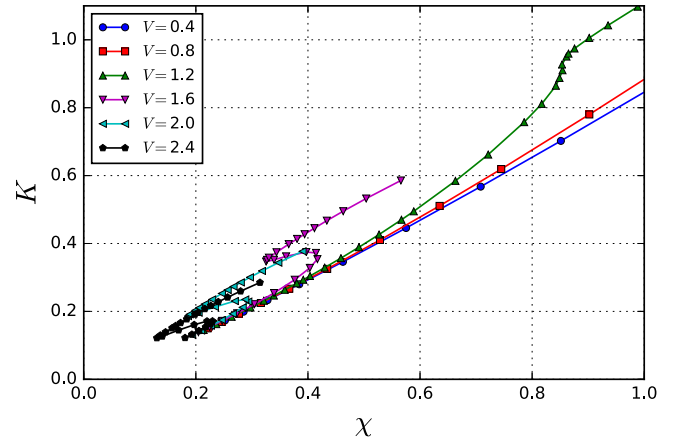


FIG. 2. The Knight shift K versus the total susceptibility χ with T as an implicit parameter. $K(\chi)$ shows counterclockwise turnaround with decreasing temperature but displays a second clockwise turnaround at lower temperature for strong hybridizations due to the continual increase of the total susceptibility in Fig. 3.

a straight line [45], $K = B_{\text{eff}} \chi + K_{0\text{eff}}$. Figure 3 illustrates the Knight-shift anomaly by comparing χ and $\tilde{K} = (K - K_{0\text{eff}})/B_{\text{eff}}$, which clearly shows the deviation between χ and \tilde{K} below a V -dependent temperature scale for a wide range of hybridizations. For large hybridization, the total susceptibility has a peak characterizing the formation of the hybridized local moment. At lower temperatures, as discussed in Fig. 1, the continual increase of the total susceptibility is attributed to both the Van Hove singularity and the mismatch of the c - f orbital occupancies. Note that the peak value decreases with increasing V , which is consistent with the trend in Fig. 2 that the turnaround point for large V precedes that for small V .

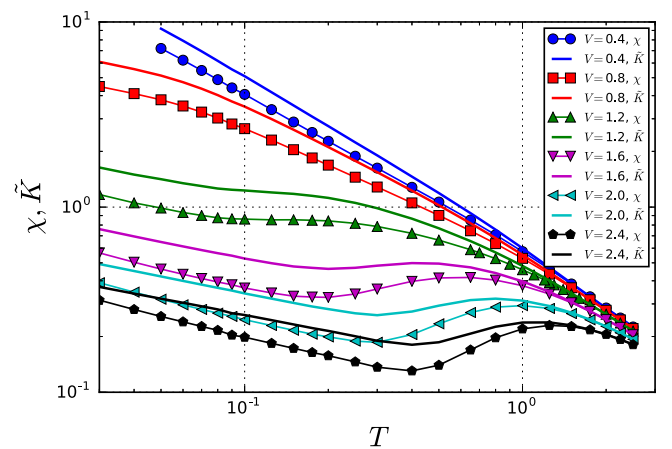


FIG. 3. The Knight-shift anomaly manifested by the deviation between the renormalized Knight shift $\tilde{K} = (K - K_{0\text{eff}})/B_{\text{eff}}$ and total susceptibility χ for $\langle n_f \rangle = 0.9$ below a certain temperature scale. The continual increase of χ originates from both the Van Hove singularity and the mismatch of the c - f orbital occupancies as discussed in Fig. 1.

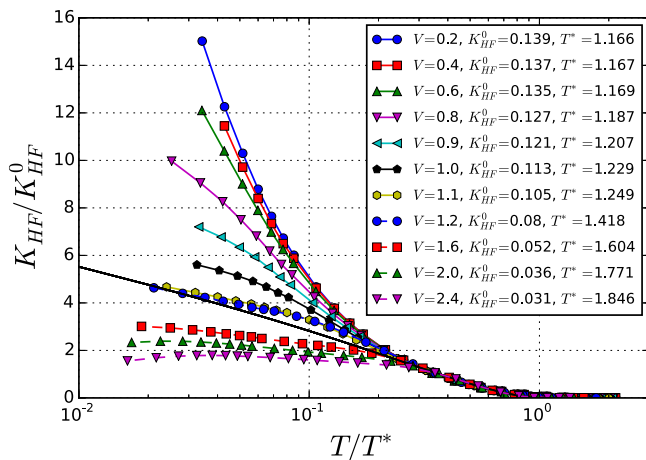


FIG. 4. Universal logarithmic scaling of K_{HF} below a V -dependent temperature T^* for a wide range of hybridization for $\langle n_f \rangle = 0.9$. K_{HF}^0 and T^* are free parameters for fitting $K_{\text{HF}}(T)$ with Eq. (5). The black curve shows the scaling function $(1 - T/T^*)^{3/2}[1 + \ln(T^*/T)]$ for comparison. T^* increases with the hybridization V , reflecting the enhancement of coherence between c - f electrons, while the prefactor K_{HF}^0 decreases with the hybridization. See text for more discussion.

IV. UNIVERSAL SCALING WITH VARYING HYBRIDIZATION AND DOPING

The Knight-shift anomaly below the V -dependent temperature scale T^* in Fig. 3 implies that the physical quantity $K_{\text{HF}} = \tilde{K} - \chi$ reflects the increasingly important role of hybridization between the f -electron spins and the conduction-electron spins. The two-fluid model [14–19] argues that below T^* the hybridization-induced heavy electrons and residual unhybridized f -local moments coexist and both contribute to the Knight shift but with different weights so that K is no longer proportional to the total susceptibility. K_{HF} strongly depends on the hybridization V (not shown here), which is reminiscent of its material dependence in experiments. One remarkable feature associated with the Knight-shift anomaly is its scaling behavior observed in a wide range of heavy-fermion materials [4], which provides strong support for the two-fluid model [17]. Empirically, K_{HF} has been found to exhibit a *universal* logarithmic divergence with decreasing temperature below T^* [16]:

$$K_{\text{HF}}(T) = K_{\text{HF}}^0(1 - T/T^*)^{3/2}[1 + \ln(T^*/T)], \quad (5)$$

where K_{HF}^0 and T^* are material-dependent constants. Figure 4 displays the scaling behavior of $K_{\text{HF}}(T)$ by fitting it near T^* with Eq. (5) using parameters K_{HF}^0 and T^* for a wide range of hybridization. The intriguing universal logarithmic scaling below a V -dependent temperature T^* provides a microscopic demonstration of the Knight-shift anomaly, suggesting that heavy-electron materials can be described in a unified way only with distinct crossover temperature T^* . In Appendix B, we discuss the results for generic n_c away from the Van Hove singularity. We fix the total occupancy $n_c + n_f$ and find that there is a charge redistribution between conduction and f electrons with temperature. However, the same universal scaling seems robust in spite of this complication.

Figure 4 reveals several noticeable features of the Knight-shift anomaly in the doped PAM. Evidently, the scaling of K_{HF} only applies between T^* and a lower temperature scale T_0 , which is consistent with experimental observations and reflects the intervention of other effects at temperatures below T_0 [17]. The low-temperature behaviors of K_{HF} differ distinctively between weak and strong hybridizations. In particular, at small V and absent antiferromagnetism, K_{HF} keeps increasing and the deviation from the scaling formula originates in part from the interplay between the residual f moments and the conduction electrons. In the presence of long-range antiferromagnetic order, the Knight-shift anomaly is typically suppressed, owing to the competition between the heavy-electron formation and the localization caused by the magnetic ordering. This is termed relocation of heavy electrons, as has been observed in CeRhIn₅, CePt₂In₇, and other heavy-fermion antiferromagnets [5,46]. In either case, the f -electron moments remain partially screened and partially localized and one expects a continuing competition between the itinerant and localized behavior, causing possible coexistence of long-range antiferromagnetism (or a spin liquid in the absence of long-range order) and unconventional superconductivity [17]. While at large V , K_{HF} is seen to saturate below T_0 , the constant behavior at low temperatures reflects complete hybridization of the f -electron moments and the ground state is a heavy Fermi liquid. Between these two regimes, one finds a minimal deviation of K_{HF} from the two-fluid scaling at an intermediate $V/t \sim 1.2$. This corresponds roughly to the quantum critical point between antiferromagnetism and the Fermi liquid, suggesting that the two-fluid scaling has less intervention by low-temperature “orders”. We note that the onset temperature T^* increases with the hybridization V , reflecting the enhancement of coherence between c - f electrons. On the other hand, the prefactor K_{HF}^0 , which is relevant to the concept of hybridization effectiveness in the two-fluid model, decreases with the hybridization. In the two-fluid model, K_{HF}^0 is inversely proportional to T^* [17], which may partially explain the change in K_{HF}^0 .

Figure 5 provides a systematic study of the Knight-shift anomaly for varying $\langle n_f \rangle$ in all three regimes of hybridizations. Similarly to the case in Fig. 4, K_{HF} displays universal scaling behavior below T^* down to a breakdown temperature T_0 . For weak hybridization, K_{HF} approaches gradually the scaling formula at low temperatures with decreasing $\langle n_f \rangle$, indicating the weakening of the local-moment effect away from half filling. For intermediate and strong hybridizations, K_{HF} below T_0 first approaches the universal scaling but then deviates again. This nonmonotonic variation with $\langle n_f \rangle$ reflects the crossover from the heavy-fermion regime ($\langle n_f \rangle = 1$) to the mixed-valence regime. In particular, it suggests two different Fermi liquid states for $\langle n_f \rangle \sim 1$ and $\langle n_f \rangle \ll 1$ at strong hybridization, probably separated by an intermediate non-Fermi liquid phase around $\langle n_f \rangle \sim 0.75$. Interestingly, for all doping levels illustrated including half filling, the onset temperature of the Knight-shift anomaly, T^* , grows rapidly with the hybridization parameter V as expected, but only weakly on $\langle n_f \rangle$ as shown in Fig. 6. This suggests that the variation of $\langle n_f \rangle$ plays a less important role in determining the magnitude of the hybridization compared to V . Figure 6 also shows the decrease of the prefactor K_{HF}^0 with $\langle n_f \rangle$ and

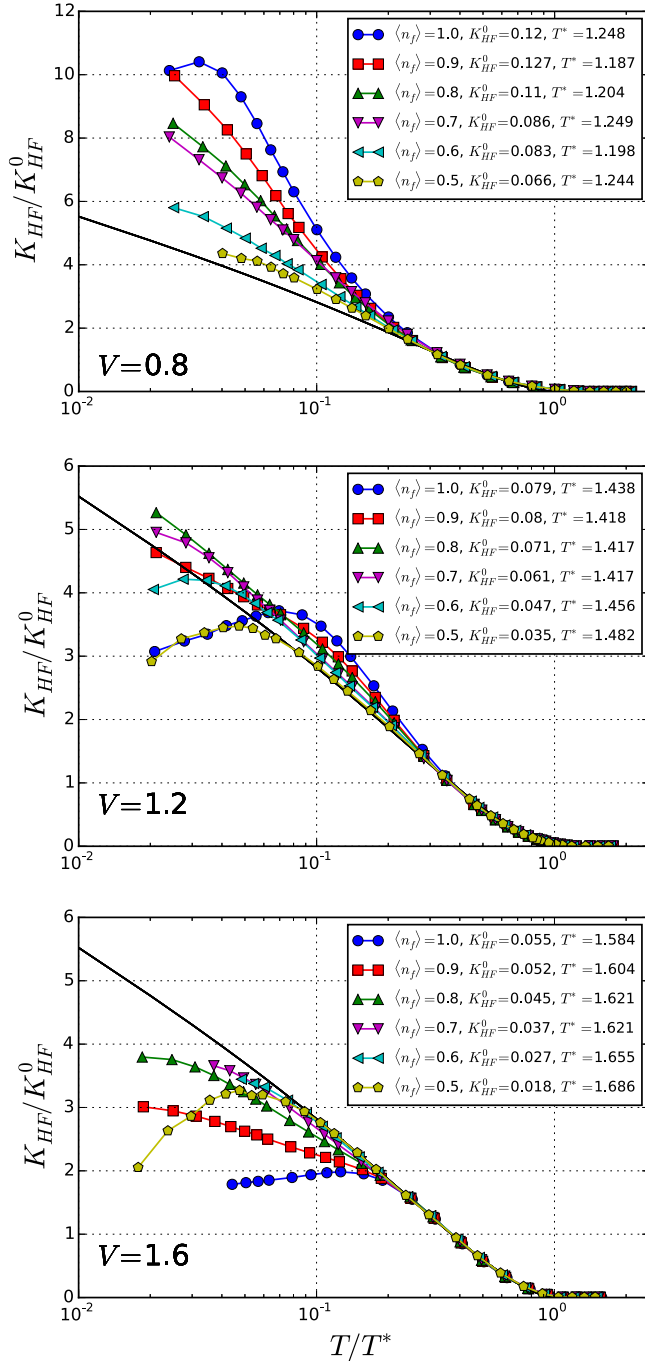


FIG. 5. Universal logarithmic scaling of K_{HF} with varying f -electron occupancy $\langle n_f \rangle$ for three hybridization regimes. The black curve shows the scaling function $(1 - T/T^*)^{3/2}[1 + \ln(T^*/T)]$ for comparison. Doping strongly modifies the behavior of K_{HF} after the scaling breakdown at low temperatures in comparison with the scaling curve. A crossover is seen around $V = 1.2$, possibly corresponding to the transition between heavy-fermion and strong mixed-valence regimes.

hybridization V , which provides a strong hint on two extreme cases, namely strong enough hybridization and/or very low $\langle n_f \rangle$, where K_{HF}^0 vanishes leading to the suppression of the Knight-shift anomaly in those systems. In fact, as argued in the two-fluid model, the crucial ingredient for the occurrence

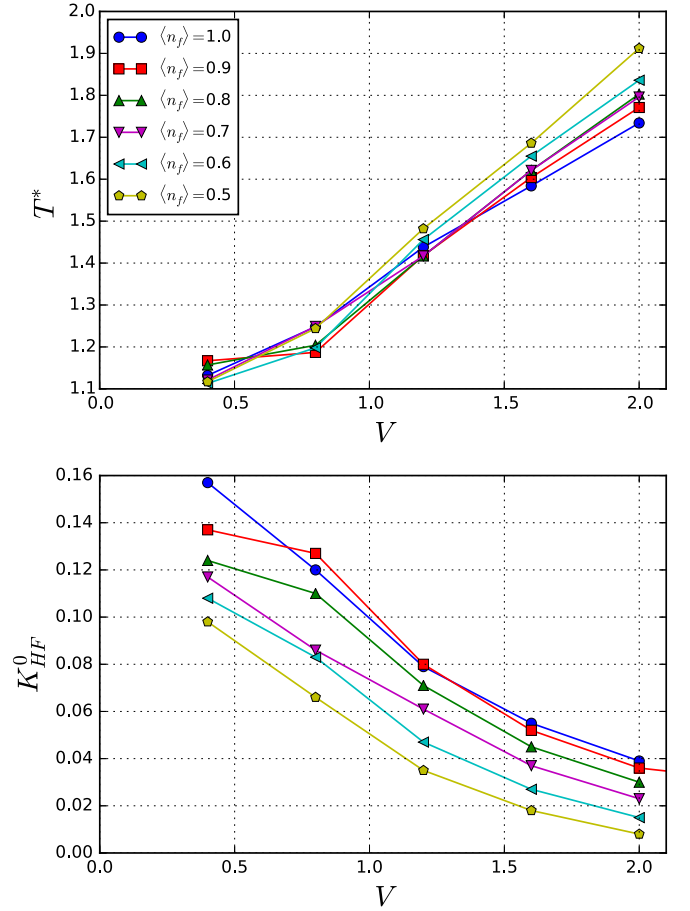


FIG. 6. Evolution of T^* and K_{HF}^0 with doping and hybridization based on the results in Fig. 4 and Fig. 5. For all doping levels including half filling, T^* grows rapidly with V but only weakly with doping. K_{HF}^0 decreases with both $\langle n_f \rangle$ and hybridization V , which implies the suppression of the Knight-shift anomaly in systems with either strong enough hybridization or very low $\langle n_f \rangle$.

of an obvious Knight-shift anomaly is the existence of two competing fluids, which is missing in both extreme cases where only one fluid dominates: the heavy electrons for strong hybridization V and the conduction electrons for low enough $\langle n_f \rangle$. Our DCA simulations confirmed the suppression of the Knight-shift anomaly in both cases.

V. COMPARISON WITH THE DENSITY OF STATES AND THE QUASIPARTICLE SCATTERING RATE

One essential piece of the two-fluid model is that the density of states (DOS) of the heavy-electron Kondo liquid has the same universal scaling form as the Knight-shift anomaly. Undoubtedly, it is important to numerically examine how these two universalities are correlated in PAM. To this end, we calculate the local density of states (DOS) for f electrons $N_f(\omega)$ via analytical continuation of the local imaginary-time Green's function $G_f(\tau) = -\sum_j \langle c_{j\pm}(\tau)c_{j\pm}^\dagger(0) \rangle$ by inverting

$$G_f(\tau) = \int_{-\infty}^{\infty} d\omega \frac{e^{-\omega\tau}}{e^{-\beta\omega} + 1} N_f(\omega) \quad (6)$$

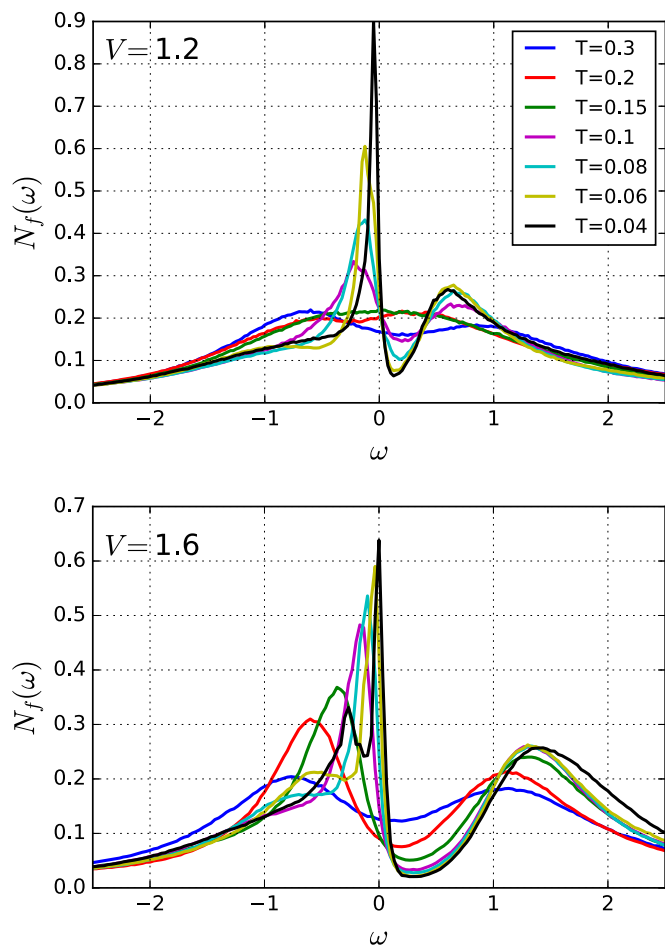


FIG. 7. Temperature evolution of f -electron local density of states for two typical hybridizations for $\langle n_c \rangle = 1.0$, $\langle n_f \rangle = 0.9$. The spectral peak shifts towards the Fermi energy with lowering T , which is accompanied by the increase of the peak height.

using the maximum-entropy method [47,48]. The investigation of the spectral properties and quasiparticle scattering rate in the PAM and/or related Kondo lattice models has been previously performed using dynamical mean field theory and related methods [27–29,35,36,49–52].

In previous two-fluid analysis of existing experimental data on CeCoIn₅ and many other heavy-fermion compounds [15], it has been suggested that T^* provides a unified temperature/energy scale for the magnetic, transport, and spectral properties, which should be reflected in the Knight shift, resistivity, and DOS, respectively. On one hand, the temperature dependence of the resistivity can be qualitatively captured by the temperature derivative of the quasiparticle scattering rate, namely the imaginary part of the local f -electron self-energy $\text{Im}\Sigma_f(\omega = 0)$. As pointed out in [49], the peak position of $-d(\text{Im}\Sigma_f)/d \ln T(\omega = 0)$ gives a good estimate of the coherence temperature in the resistivity. On the other hand, previous calculations of CeIrIn₅ [16,49] have also shown that the universal scaling can be manifested in the temperature scaling of the quasiparticle DOS peak.

Figure 7 illustrates the temperature evolution of the f -electron local density of states $N_f(\omega)$ for two characteristic hybridizations and $\langle n_f \rangle = 0.9$. The right shift of the spectral

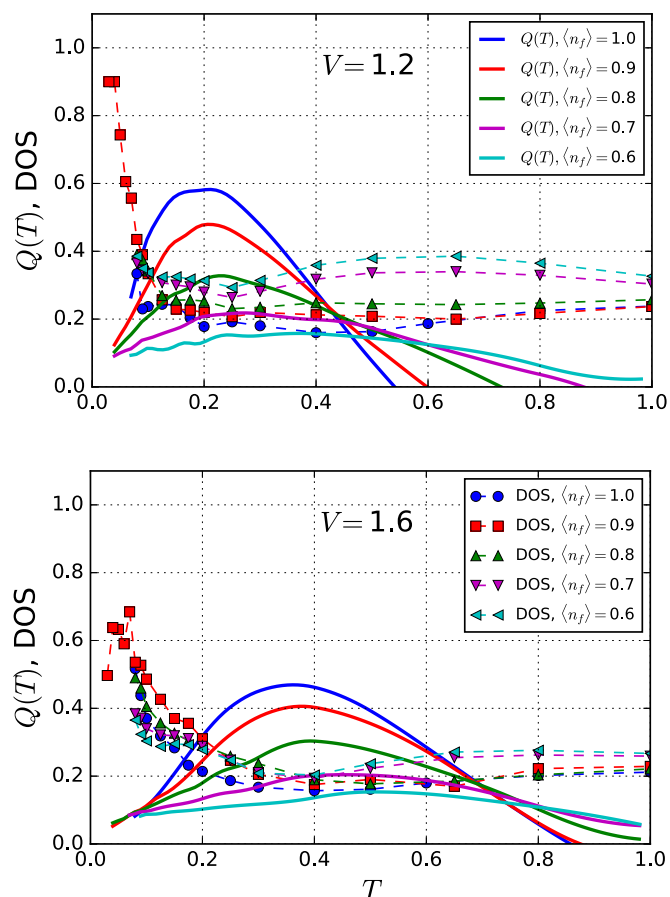


FIG. 8. The peak temperature of the temperature derivative of the quasiparticle scattering rate $Q(T)$ (solid lines) and the temperature scale below which the peak height of the local DOS of f electrons (dashed lines with markers) shows a rapid increase roughly agree, especially for small dopings and strong hybridizations. This temperature scale grows with V but is much lower than the onset temperature T^* of the Knight-shift anomaly.

peak with lowering T reflects the gradual formation of the hybridization gap, which is accompanied by the increase of the peak height. Figure 8 further compares the temperature derivative of quasiparticle scattering rate defined as

$$Q(T) \equiv \frac{-d[\text{Im}\Sigma_f(i\omega = \pi T)]}{d \ln T} \quad (7)$$

(solid lines) and the peak height of $N_f(\omega)$ (dashed lines with markers) with varying $\langle n_f \rangle$ [53]. The peak of $Q(T)$ roughly resides at the temperature scale below which the peak height of local DOS shows a rapid increase (more clear for small dopings and strong hybridizations). Although apparently this temperature scale grows with V , it is much lower than the onset temperature T^* of the Knight-shift anomaly, which is in distinct difference from the experimental observation in CeCoIn₅ and many other compounds. However, we should note that there do exist a few examples such as CeCu₂Si₂ and UBe₁₃, where the resistivity peak appears at a much lower temperature than T^* estimated from the NMR Knight shift [15]. There are two possible reasons for this discrepancy: either accidental due to the involvement of some other effects, or representing a particular kind of heavy-fermion physics

different from that of CeCoIn_5 . In either case, it would be important to clarify the conditions for which the three quantities exhibit similar/different T^* . Possible extensions would be to perform calculations taking into account additional bosonic excitations such as spin fluctuations or phonons, which might lead to dynamical renormalization of the hybridization V and a large reduction of the coherence temperature [54]. This might give an additional control parameter to tune T^* for fitting with the experimental findings.

VI. CONCLUSION

We extend previous theoretical study of the NMR Knight shift in the half-filled periodic Anderson model to the doped case using the DCA method. Our simulations show that the universal scaling of the Knight-shift anomaly persists in the moderate doping levels and hybridization regime and represents a robust property of the Anderson lattice. Our work provides a plausible basis for developing a microscopic understanding of the phenomenological two-fluid model. However, it also indicates that some essential physics is missing in the current model calculations, as it cannot reproduce the common T^* for the magnetic, transport, and spectral properties observed in CeCoIn_5 and many other heavy-fermion compounds. This reveals a missing piece in explaining the two-fluid phenomenology in the current model calculations, which may be the key for a thorough solution of the heavy-fermion problem.

ACKNOWLEDGMENTS

We acknowledge the Swiss National Supercomputing Center (CSCS) for computing facility support. Y.Y. was supported by the National Natural Science Foundation of China (Grant No. 11522435) and the Youth Innovation Promotion Association CAS.

APPENDIX A: COMPARISON OF LOCAL SUSCEPTIBILITIES BETWEEN DQMC AND THE DCA IN THE HALF-FILLED PAM

The main text aims to extend the previous DQMC study on the half-filled PAM [21] to the generally doped PAM using the DCA method. Therefore, it is valuable to compare the three orbital-dependent local susceptibilities in the half-filled case from two numerical methods.

Adopting a characteristic common DQMC lattice size and DCA cluster size 4×4 , Fig. 9 illustrates the excellent agreement between DQMC and the DCA of all three local susceptibilities at high temperatures for half filling. Nevertheless, at lower temperatures, they deviate for weak hybridization $V = 0.8$ because the presence of the nonlocal antiferromagnetic correlation is treated in essentially different ways. The DCA incorporates the host outside of the cluster in a self-consistent mean-field manner, while DQMC normally considers the bulk system by employing the periodic boundary conditions. It is well known that DQMC simulations exhibit strong finite-size effects for weak correlations or when the itinerancy of conduction electrons is strong [55]. Figure 9 shows the approach of DQMC's local susceptibilities to

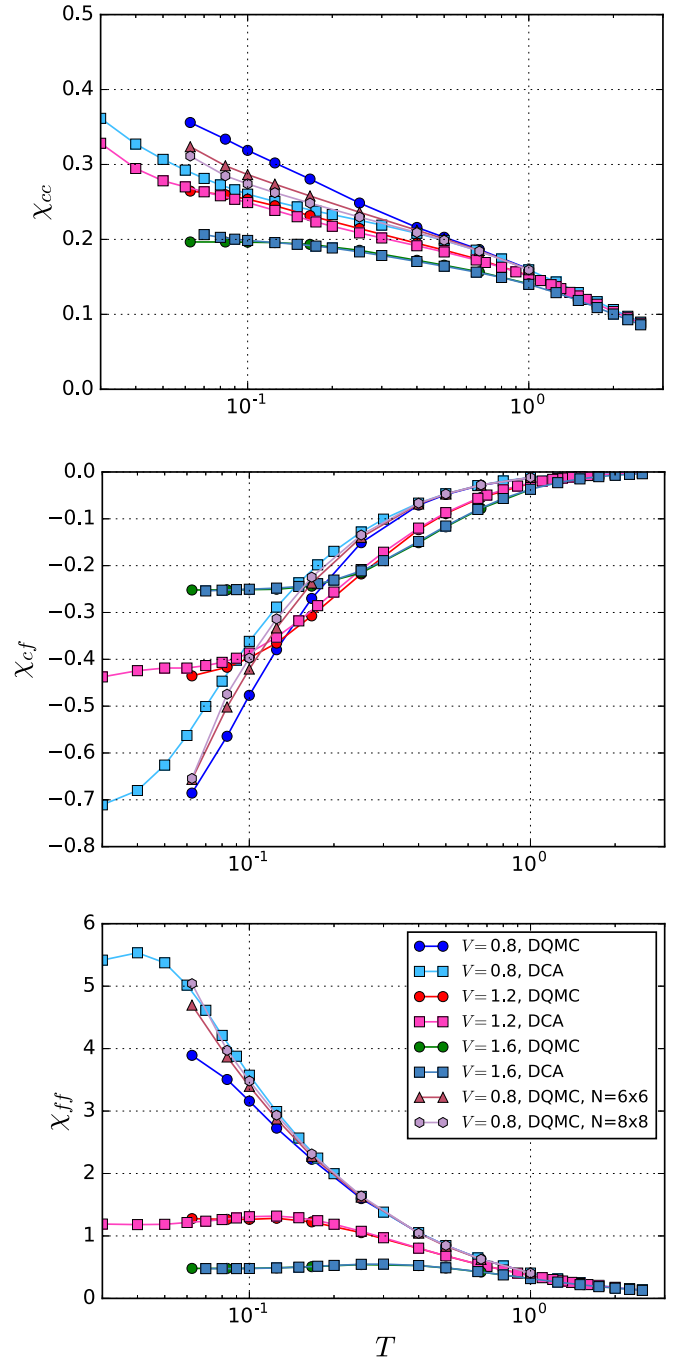


FIG. 9. Comparison of local susceptibilities in the half-filled PAM from DQMC and DCA simulations, which show excellent agreement at high temperatures. The deviation at low temperature for weak hybridization is due to the finite-size effect in DQMC and can be recovered by simulating larger lattice size. The Van Hove singularity induced continuing increase of χ_{cc} shows up even for large V due to the mean-field host in the DCA to effectively enhance the itinerancy of conduction electrons.

DCA curves via two larger lattice sizes, $N = 6 \times 6$, 8×8 . Apparently, the deviation between DQMC and DCA curves is expected to completely vanish in the limit of the infinite DQMC lattice or DCA cluster size. As expected, this difference is hidden for strong hybridization $V = 1.6$ due to the locality

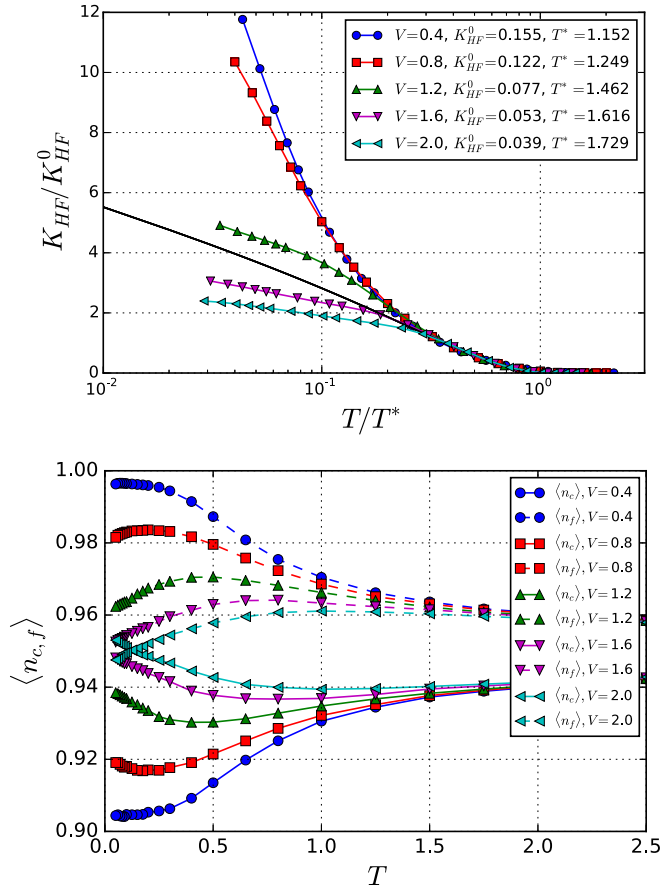


FIG. 10. Top: Universal scaling of the Knight-shift anomaly for fixed total orbital occupancy $\langle n_c + n_f \rangle = 1.9$. T^* and K_{HF}^0 are close to the values in Fig. 4, indicating the robustness of the universality against the orbital occupancy distribution. Bottom: Orbital occupancy as a function of temperature indicates that the hole doping mainly affects the conduction-electron occupancy at low temperatures, especially for weak hybridization.

of the singlet formation via hybridization so that both DQMC's finite-size effects and the DCA's dependence on cluster size can be neglected.

One issue discussed in the main text is the Van Hove singularity manifested in χ_{cc} especially for weak hybridization due to the half-filled conduction electrons. Figure 9 clearly shows that the associated continuing increase of χ_{cc} at low temperatures already occurs at $\langle n_f \rangle = 1.0$ for $V = 0.8$ and even for strong hybridization $V = 1.6$ in the DCA, while the flatness of χ_{cc} at low temperatures is correctly captured in DQMC for large V . This is largely due to the mean-field host coupled self-consistently with the DCA cluster so that the itinerancy of conduction electrons is effectively enhanced. More discussions on other features of magnetic susceptibilities of the half-filled PAM can be found in Ref. [21].

APPENDIX B: FIXED TOTAL ORBITAL OCCUPANCY

As mentioned in the main text, we adopt the fixed $\langle n_c \rangle \sim 1$ but varying $\langle n_f \rangle$ via tuning an ‘‘artificially’’ orbital-dependent chemical potential $\mu_{c,f}$ in order to explicitly examine the impact of f -orbital occupancy. As discussed in Fig. 1 and Appendix A, $\langle n_c \rangle \sim 1$ leads to the Van Hove singularity in the density of states causing the lack of Pauli-like behavior in $\chi_{cc}(T)$ for small V . Hence, it is interesting to check our major result, namely the universal scaling of the Knight-shift anomaly in Fig. 4, in more generic settings.

The upper panel of Fig. 10 shows that the universal scaling of the Knight-shift anomaly persists for fixed total orbital occupancy $\langle n_c + n_f \rangle = 1.9$ via tuning a ‘‘global’’ chemical potential $\mu = \mu_c = \mu_f$. Remarkably, even T^* and K_{HF}^0 are quite close to the values in Fig. 4. The bottom panel shows the orbital occupancy as a function of temperature, which indicates that the hole doping mainly affects the conduction-electron occupancy at low temperatures, especially for weak hybridization, while the singlet formation for strong hybridization results in more even distribution between orbitals. Figure 10 provides evidence of the robustness of the universal Knight-shift anomaly against the orbital occupancy distribution, supporting the major results in the main text.

- [1] G. Stemann, C. Pépin, and M. Lavagna, *Phys. Rev. B* **50**, 4075 (1994).
- [2] J. Thoma, S. Tewari, J. Ruvalds, and C. T. Rieck, *Phys. Rev. B* **51**, 15393 (1995).
- [3] A. S. Moskvin, *Phys. Rev. B* **75**, 054505 (2007).
- [4] N. J. Curro, B.-L. Young, J. Schmalian, and D. Pines, *Phys. Rev. B* **70**, 235117 (2004).
- [5] K. R. Shirer, A. C. Shockley, A. P. Dioguardi, J. Crocker, C. H. Lin, N. apRoberts-Warren, D. M. Nisson, P. Klavins, J. C. Cooley, Y.-F. Yang, and N. J. Curro, *Proc. Natl. Acad. Sci. USA* **109**, E3067 (2012).
- [6] Y. P. Wu, D. Zhao, A. F. Wang, N. Z. Wang, Z. J. Xiang, X. G. Luo, T. Wu, and X. H. Chen, *Phys. Rev. Lett.* **116**, 147001 (2016).
- [7] T. Park, F. Ronning, H. Q. Yuan, M. B. Salamon, R. Movshovich, J. L. Sarrao, and J. D. Thompson, *Nature (London)* **440**, 65 (2006).
- [8] B.-L. Young, R. R. Urbano, N. J. Curro, J. D. Thompson, J. L. Sarrao, A. B. Vorontsov, and M. J. Graf, *Phys. Rev. Lett.* **98**, 036402 (2007).
- [9] M. Kenzelmann, Th. Strässle, C. Niedermayer, M. Sgrist, B. Padmanabhan, M. Zolliker, A. D. Bianchi, R. Movshovich, E. D. Bauer, J. L. Sarrao, and J. D. Thompson, *Science* **321**, 1652 (2008).
- [10] N. J. Curro, *Rep. Prog. Phys.* **72**, 026502 (2009).
- [11] E. Kim, M. Makivic, and D. L. Cox, *Phys. Rev. Lett.* **75**, 2015 (1995).
- [12] T. Ohama, H. Yasuoka, D. Mandrus, Z. Fisk, and J. L. Smith, *J. Phys. Soc. Jpn.* **64**, 2628 (1995).
- [13] F. Mila and T. M. Rice, *Phys. Rev. B* **40**, 11382(R) (1989).
- [14] S. Nakatsuji, D. Pines, and Z. Fisk, *Phys. Rev. Lett.* **92**, 016401 (2004).
- [15] Y.-f. Yang, Z. Fisk, H.-O. Lee, J. D. Thompson, and D. Pines, *Nature (London)* **454**, 611 (2008).

- [16] Y.-f. Yang and D. Pines, *Phys. Rev. Lett.* **100**, 096404 (2008).
- [17] Y.-f. Yang and D. Pines, *Proc. Natl. Acad. Sci. USA* **109**, E3060 (2012).
- [18] G. Lonzarich, D. Pines, and Y.-f. Yang, *Rep. Prog. Phys.* **80**, 024501 (2017).
- [19] Y.-f. Yang, *Rep. Prog. Phys.* **79**, 074501 (2016).
- [20] J. Gan, P. Coleman, and N. Andrei, *Phys. Rev. Lett.* **68**, 3476 (1992).
- [21] M. Jiang, N. J. Curro, and R. T. Scalettar, *Phys. Rev. B* **90**, 241109(R) (2014).
- [22] N. J. Curro, *Rep. Prog. Phys.* **79**, 064501 (2016).
- [23] W. Wu and A.-M.-S. Tremblay, *Phys. Rev. X* **5**, 011019 (2015).
- [24] M. Jarrell, Th. Maier, C. Huscroft, and S. Moukouri, *Phys. Rev. B* **64**, 195130 (2001).
- [25] T. Maier, M. Jarrell, T. Pruschke, and M. H. Hettler, *Rev. Mod. Phys.* **77**, 1027 (2005).
- [26] P. Sun and G. Kotliar, *Phys. Rev. Lett.* **95**, 016402 (2005).
- [27] L. De Leo, M. Civelli, and G. Kotliar, *Phys. Rev. B* **77**, 075107 (2008).
- [28] A. Amaricci, G. Sordi, and M. J. Rozenberg, *Phys. Rev. Lett.* **101**, 146403 (2008).
- [29] D. E. Logan, M. R. Galpin, and J. Mannouch, *J. Phys.: Condens. Matter* **28**, 455601 (2016).
- [30] A. Amaricci, L. de' Medici, and M. Capone, [arXiv:1612.09096](https://arxiv.org/abs/1612.09096).
- [31] S. Acharya, M. S. Laad, and A. Taraphder, *J. Phys.: Conf. Ser.* **759**, 012037 (2016).
- [32] M. A. Majidi, D. G. S. P. Doluweera, B. Moritz, P. R. C. Kent, J. Moreno, and M. Jarrell, [arXiv:0710.5937](https://arxiv.org/abs/0710.5937).
- [33] T. Misawa, J. Yoshitake, and Y. Motome, *Phys. Rev. Lett.* **110**, 246401 (2013); S. Hayami, T. Misawa, and Y. Motome, *JPS Conf. Proc.* **3**, 016016 (2014).
- [34] K. Byczuk, W. Hofstetter, U. Yu, and D. Vollhardt, *Eur. Phys. J.: Spec. Top.* **180**, 135 (2010).
- [35] A. Koga and P. Werner, *J. Phys. Soc. Jpn.* **79**, 114401 (2010).
- [36] M. W. Aulbach, F. F. Assaad, and M. Potthoff, *Phys. Rev. B* **92**, 235131 (2015).
- [37] H. Tsunetsugu, M. Sigrist, and K. Ueda, *Rev. Mod. Phys.* **69**, 809 (1997).
- [38] A. Georges, G. Kotliar, W. Krauth, and M. J. Rozenberg, *Rev. Mod. Phys.* **68**, 13 (1996).
- [39] E. Gull, A. J. Millis, A. I. Lichtenstein, A. N. Rubtsov, M. Troyer, and P. Werner, *Rev. Mod. Phys.* **83**, 349 (2001).
- [40] E. Gull, P. Werner, O. Parcollet, and M. Troyer, *Europhys. Lett.* **82**, 57003 (2008).
- [41] P. Staar, T. Maier, and T. C. Schulthess, *Phys. Rev. B* **89**, 195133 (2014).
- [42] P. Staar, M. Jiang, U. R. Hähner, T. C. Schulthess, and T. A. Maier, *Phys. Rev. B* **93**, 165144 (2016).
- [43] A. M. Clogston and V. Jaccarino, *Phys. Rev.* **121**, 1357 (1961).
- [44] We adopt $B = 1$ so that only A/B is varied. It is found that the specific values of hyperfine interactions A and B do not modify any results qualitatively.
- [45] The high-temperature range for the linear fit is determined in the sense of the least-squares fit.
- [46] N. apRoberts-Warren, A. P. Dioguardi, A. C. Shockley, C. H. Lin, J. Crocker, P. Klavins, D. Pines, Y.-F. Yang, and N. J. Curro, *Phys. Rev. B* **83**, 060408(R) (2011).
- [47] J. E. Gubernatis, M. Jarrell, R. N. Silver, and D. S. Sivia, *Phys. Rev. B* **44**, 6011 (1991).
- [48] Note that as a tricky and ill-defined problem that is sensitive to the quality of the Green's function data, the maximum-entropy method introduces ambiguity into the reliability of the spectral function. To be precise, we also managed to obtain the cluster momentum dependent spectral function $N_f(\mathbf{K}, \omega)$ via the analytical continuation of $G_f(\mathbf{K}, \tau)$ so that $N_f(\omega) = \sum_{\mathbf{K}} N_f(\mathbf{K}, \omega)$. We found that this much more time-consuming procedure does not significantly improve the quality of $N_f(\omega)$, in particular the temperature scale below which the peak height of $N_f(\omega)$ starts growing rapidly.
- [49] J. H. Shim, K. Haule, and G. Kotliar, *Science* **318**, 1615 (2007).
- [50] L. C. Martin, M. Bercx, and F. F. Assaad, *Phys. Rev. B* **82**, 245105 (2010).
- [51] R. Peters, S. Hoshino, N. Kawakami, J. Otsuki, and Y. Kuramoto, *Phys. Rev. B* **87**, 165133 (2013).
- [52] R. Dong, J. Otsuki, and S. Y. Savrasov, *Phys. Rev. B* **87**, 155106 (2013).
- [53] The cases for small hybridizations, e.g., $V = 0.8$, are not shown here due to the noisy DOS data obtained by maximum-entropy method.
- [54] M. Raczkowski, P. Zhang, F. F. Assaad, T. Pruschke, and M. Jarrell, *Phys. Rev. B* **81**, 054444 (2010).
- [55] M. Jiang and T. C. Schulthess, *Phys. Rev. B* **93**, 165146 (2016).